

# POLITECNICO DI TORINO

Corso di Laurea in Ingegneria Aerospaziale



Tesi di Laurea

*Vortex formation as driver of bio-inspired propulsion*

**Relatore:**

Prof.ssa Stefania Scarsoglio

**Candidato:**

Luca Rinaldi

---

Anno Accademico 2021/2022  
Sessione di Laurea Luglio 2022



# Contents

<b>1</b>	<b>Introduction</b>	<b>7</b>
1.1	History of Vortex Dynamics . . . . .	7
1.2	Purpose and Outline . . . . .	8
<b>2</b>	<b>Theory</b>	<b>9</b>
2.1	Reminders of Fluid Dynamics . . . . .	9
2.2	Optimal Vortex Formation . . . . .	13
2.2.1	Definitions . . . . .	13
2.2.2	Limits and Constraints . . . . .	13
2.2.3	Preliminary Studies . . . . .	14
<b>3</b>	<b>Applications</b>	<b>17</b>
3.1	Self-Propelled Vehicles Propulsion . . . . .	17
3.1.1	Analytical Model . . . . .	17
3.1.2	Experimental Setup and Methods . . . . .	19
3.1.3	Enhancement on Vehicle Performance . . . . .	22
3.2	Biologic Propulsion Mechanisms . . . . .	23
3.2.1	Squids, Jellyfish and Salps . . . . .	23
3.2.2	Fish . . . . .	24
3.2.3	Measurements . . . . .	26
3.3	Blood Flow in the cardiac left ventricle . . . . .	27
3.3.1	Results . . . . .	27
3.3.2	Methods . . . . .	28
<b>4</b>	<b>Discussion</b>	<b>31</b>
4.1	Outlook . . . . .	31
4.2	Pros and Cons . . . . .	31
4.3	Recommendations of Future Work . . . . .	32



# List of Figures

2.1	Boundary layer velocity profile [2]. . . . .	10
2.2	Visualization of vortex rings for (a) $T = 2$ , (b) $T = 3.8$ , (c) $T = 14.5$ [4]. . . . .	14
2.3	Normalized average thrust per pulse measurements [4]. . . . .	14
2.4	Example of a piston-cylinder apparatus used by Gharib [3]. . . . .	15
3.1	Submarine (in black) and associated control volume (dashed lines) [5]. . . . .	18
3.2	Schematic diagram of vehicle components including horizontal traverse [5]. . . . .	19
3.3	PLIF images of the near-wake of the vehicle during steady (a) and unsteady (b) propulsion [5]. . . . .	20
3.4	Typical output of a DPIV measurement [6]. . . . .	21
3.5	LDV assembly mounted onto the vehicle traverse [5]. . . . .	22
3.6	The water flow through a salp [7]. . . . .	24
3.7	Vortex wakes of two different swimming fishes produced with pectoral fins [7]. . . . .	25
3.8	Lateral view of sunfish swimming with the caudal fin [7]. . . . .	25
3.9	Three-dimensional in-vivo intra-cardiac vortex flow [11]. . . . .	27
3.10	Vortex formation time in adult humans from blind test and those with DCM [11]. . . . .	28



# Chapter 1

## Introduction

### 1.1 History of Vortex Dynamics

The subject of vortex dynamics can be considered to have started from the paper of Hermann Ludwig Ferdinand Helmholtz (1821-1894) about a century and a half ago [1]. Within this article, Helmholtz laid the groundwork for the three laws of vortex motion, in a form very similar to the one in which we know them today.

Before this historic article, the integrals of the hydrodynamic equations were exclusively determined on the assumption that the Cartesian components of the velocity of each fluid particle are partial first derivatives with respect to the Cartesian coordinates of a certain function, the velocity potential. This assumption is valid so long as the motion of the fluid results from the action of forces that have a potential of their own. Helmholtz eliminated this limitation, and took into account the possible friction between different elements of the fluid or between the fluid and a solid boundary.

When seeing the fluid motion as a velocity vector field, **vorticity** describes the circulation of that said velocity field and is defined by the equation:

$$\vec{\omega} = \nabla \times \vec{U} \quad (1.1)$$

$\vec{\omega}$  is a vector that describes the local rotary motion at a point in the fluid, as would be perceived by an observer that moves along with it, while  $\vec{U}$  represents the flow velocity. On a purely conceptual level, one could think of observing the vorticity by inserting a ball in the point considered and observing the rotational motion that this assumes around its center.

Vortex structures can be formed via the phenomenon known as boundary layer separation which can occur when a fluid moves over a surface and experiences a rapid acceleration from the fluid velocity to zero due to the no-slip condition<sup>1</sup>. When the boundary layer does grow beyond this critical boundary layer thickness then separation will occur which will generate vortices.

The properties of vorticity have gained increasing attention in the past century due to its nature to highlight turbulence where the most complex motion happens especially as they

---

<sup>1</sup>At a solid boundary, the fluid will have zero velocity relative to the boundary

were revealed by simulations and more accurate experiments. It is precisely the area of high vorticity where the fluid twists the most that is the most difficult to describe and these areas have significant effects on the motion of any fluid as the fluid around circulations moves much faster.

## 1.2 Purpose and Outline

Given the existence of the phenomenon of the vortex formation, in this thesis we will analyze the optimal formation of the latter. Indeed, many internal flows are characterized by flow separation and subsequent vortex shedding.

Thanks to the concept of optimal vortex formation, which will be extensively analyzed later, we will try to better understand the diversity of methods used in nature to create propulsion, so that these can be an inspiration for engineering solutions of various kinds. Our purpose is to find a unifying perspective from which to examine the diversity of solutions used in nature to achieve effective transport and transfer mass, momentum and energy in fluids.

In chapter 2, therefore, some fundamental fluid dynamics aspects are recalled and then the main parameters and concepts that characterize the phenomenon of optimal vortex formation are introduced to allow an adequate understanding of the applications treated in the following chapter.

In fact, in chapter 3, it was decided to report the analysis of three different applications linked to the optimal vortex formation. The first is more focused on the engineering aspect of the improvement of propulsion for self-propelled vehicles, the second is, instead, related to a study of the motion of living organisms that use the production of vortices as the engine of their movement, while, finally, the last one focuses on an area that combines fluid dynamics and biomedical, in the concrete hope of being able to exploit these topics of study to monitor the heart health of patients in time.

In conclusion, the aim of the last chapter is to make a reflection to summarize and provide a broader perspective of the steps forward that have been made in this research field, focusing on what may be the possible developments of the different applications in the near future.

# Chapter 2

## Theory

### 2.1 Reminders of Fluid Dynamics

#### Reynolds Number

The dimensionless **Reynolds number** plays a prominent role in foreseeing the patterns in a fluid's behavior. The Reynolds number, referred to as  $Re$ , is used to determine whether the fluid flow is **laminar** or **turbulent**. Reynolds number is the ratio of inertial (resistant to change or motion) forces to viscous (heavy and gluey) forces and it's given by:

$$Re = \frac{\rho UL}{\mu} = \frac{\rho UL}{\mu} \quad (2.1)$$

where:

- $\rho$  is the fluid density [ $\frac{kg}{m^3}$ ]
- $L$  is the characteristics linear dimension [ $m$ ]
- $U$  is the flow speed [ $\frac{m}{s}$ ]
- $\mu$  is the dynamic viscosity of the fluid [ $\frac{kg}{m \cdot s}$ ]
- $\nu$  is the cinematic viscosity of the fluid [ $\frac{m^2}{s}$ ]

#### Strouhal Number

The **Strouhal number**, referred to as  $St$ , represents the ratio of inertial forces due to the local acceleration of the flow to the inertial forces due to the convective acceleration. It's a dimensionless number describing oscillating flow mechanisms and given by the following equation:

$$St = \frac{fL}{U} \quad (2.2)$$

where:

- $f$  is the frequency of vortex shedding [Hz]

- $L$  is the characteristics linear dimension [ $m$ ]
- $U$  is the flow speed [ $\frac{m}{s}$ ]

## Boundary Layer Theory

As an object moves through a fluid, or as a fluid moves past an object, the molecules of the fluid near the object are disturbed and move around the object. Aerodynamic forces are generated between the fluid and the object.

The molecules right next to the surface stick to the surface, while ones just above the surface are slowed down in their collisions with the others sticking to the surface. These molecules in turn slow down the flow just above them. The farther one moves away from the surface, the fewer the collisions affected by the object surface. This creates a thin layer of fluid near the surface in which the velocity changes from zero at the surface to the free stream value away from the surface.

That's called **boundary layer** because it occurs on the boundary of the fluid and there are two different types of boundary layer flow: **laminar** and **turbulent**.

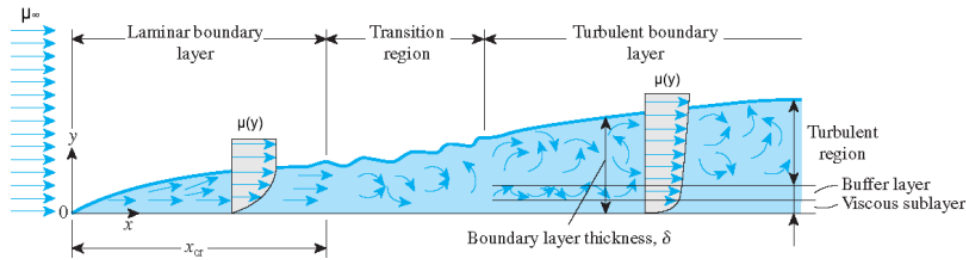


Figure 2.1: Boundary layer velocity profile [2].

## Governing Equations

The flow of a viscous fluid is governed by conservation of mass, conservation of momentum and conservation of energy.

In the most general form, the fluid motion is governed by the time-dependent three-dimensional compressible Navier-Stokes system of equations. For a viscous Newtonian, isotropic fluid, the strong conservation form of the Navier-Stokes system of equations in compact differential form can be written as:

$$\begin{cases} \frac{\partial \rho}{\partial t} + \nabla \cdot (\rho \mathbf{U}) = 0 \\ \rho \left( \frac{\partial \mathbf{U}}{\partial t} + \mathbf{U} \cdot \nabla \mathbf{U} \right) = -\nabla p + \nabla \cdot \boldsymbol{\tau} + \rho \mathbf{g} \\ \rho \left( \frac{\partial E}{\partial t} + \mathbf{U} \cdot \nabla E \right) = -\nabla \cdot (p \mathbf{U}) + \nabla \cdot (k \nabla T) + \nabla \cdot (\boldsymbol{\tau} \cdot \mathbf{U}) + \rho \mathbf{g} \cdot \mathbf{U} + q_v \end{cases}$$

where:

- $\boldsymbol{\tau}$  is the stress tensor due to viscosity

- $g$  represents the external forces
- $k$  is the thermal conductivity of the fluid
- $q_v$  stays for external heat addition

The system of equations is closed by the **state equation** and **thermodynamic relations**. The complexity of these equations is such that the Clay Mathematics Institute has called this one of the seven most important open problems in mathematics and has offered a US 1\$ million prize for a solution or a counterexample.

Precisely for this reason, the only possibility nowadays to obtain a solution from this set of equations is to adopt a numerical approximation strategy. Therefore, the three most used approaches are listed below, in increasing order of difficulty:

1. Reynolds-Averaged Navier–Stokes equations (**RANS**)
2. Large Eddy Simulation (**LES**)
3. Direct Numerical Simulation (**DNS**)

**RANS** The Reynolds-Averaged Navier–Stokes equations (RANS equations) are time averaged equations of motion for fluid flow. The idea behind the equations is the "Reynolds decomposition", whereby an instantaneous quantity is decomposed into its time-averaged and fluctuating quantities, an idea first proposed by Osborne Reynolds.

So, RANS is a numerical method to model a turbulent flow wherein the flow quantities are decomposed into their time-averaged and fluctuating components. Then, the averaging of Navier-Stokes equations yields a nonlinear Reynolds stress term that requires additional modeling to fully resolve the system known as turbulence model. It means that most, if not all, RANS turbulence models are based on empirical observations.

**LES** Large eddy simulation (LES) is a mathematical model for turbulence used in computational fluid dynamics. It was initially proposed in 1963 by Joseph Smagorinsky to simulate atmospheric air currents. LES is currently applied in a wide variety of engineering applications, including combustion, acoustics, and simulations of the atmospheric boundary layer. The simulation of turbulent flows by numerically solving the Navier–Stokes equations requires resolving a very wide range of time and length scales, all of which affect the flow field. The principal idea behind LES is to reduce the computational cost by ignoring the smallest length scales, which are the most computationally expensive to resolve, via low-pass filtering of the Navier–Stokes equations.

**DNS** Direct numerical simulation (DNS) is used to solve instantaneous Navier–Stokes equations, resolving all scales, down to the smallest dissipation scales, without using any models. It can give the most accurate results, with high spatial and temporal resolution, which cannot even be given by measurements. However, its computer requirements are extremely high, and increase rapidly with Reynolds number. That's why its application is

limited to low-Reynolds number flows and small-size computation domains. In fact, currently, DNS cannot be used to simulate practical high-Reynolds-number complex flows. The computational cost of DNS is very high, even at low Reynolds numbers. For the Reynolds numbers encountered in most industrial applications, the computational resources required by a DNS would exceed the capacity of the most powerful computers currently available. However, direct numerical simulation is a useful tool in fundamental research in turbulence. Using DNS it is possible to perform "numerical experiments", and extract from them information difficult or impossible to obtain in the laboratory, allowing a better understanding of the physics of turbulence.

## 2.2 Optimal Vortex Formation

Locomotion in water and air occurs in the Reynolds number regime  $Re > 10^2$  in which the **formation and shedding of coherent vortices** are predominant.

In addition to that, many internal flows in biological systems are characterized by flow separation and subsequent vortex shedding.

### 2.2.1 Definitions

The first step in order to define **optimal vortex formation** is to parametrize the vortex formation process.

To do that, we must introduce a **dimensionless vortex formation time**  $\hat{T}$ , defined as:

$$\hat{T} = \frac{C\Gamma}{D\Delta U} \quad (2.3)$$

where:

- $C$  is a constant factor that depends on the physical configuration of the vortex generator
- $\Gamma$  is the circulation or instantaneous vortex strength [ $\frac{m^2}{s}$ ]
- $D$  is the characteristics length scale of the shear layer feeding the vortex [ $m$ ]
- $\Delta U = (U - U_{ambient})$  is the shear layer strength [ $\frac{m}{s}$ ]

More specifically,  $C$  is given by the inverse of the dimensionless vorticity flux  $\frac{d\Gamma}{dt}$  from a given vortex generator configuration. Taking a piston-cylinder one,  $\frac{d\Gamma}{dt} \approx \frac{1}{2}$ , so that  $C = 2$ . The circulation  $\Gamma$  generated by the piston-cylinder apparatus could be approximated using the **slug model**, which is based on the following hypothesis: within the boundary layer of thickness  $\delta \ll D$ , the wall-normal velocity component  $v$  is much smaller than the streamwise component  $u$ . Under these conditions, we may write the circulation as:

$$\Gamma \approx \frac{1}{2}U^2T \quad (2.4)$$

Combining (2.3) and (2.4) we arrive at a dimensionless vortex formation timescale based on the physical parameters of the vortex generator:

$$\hat{T} = \frac{UT}{D} \quad (2.5)$$

where the letter  $T$  denotes the final dimensional time at the end of the process.

### 2.2.2 Limits and Constraints

The process of vortex ring formation has been almost entirely studied for short dimensionless vortex formation times  $\hat{T} < 4$ . In fact, in 1998 Gharib et al. [3] examined the vortex formation process for longer times,  $\hat{T} > 4$ , and observed a **robust limit** on the maximum

growth of vortex rings formed using a piston-cylinder apparatus.

Vortex ring accepts the vorticity flux from the piston-cylinder apparatus until a dimensionless formation time of  $\hat{T} \approx 4$  is reached. Beyond this time, additional vorticity flux is rejected by the vortex ring and instead forms secondary vortices.

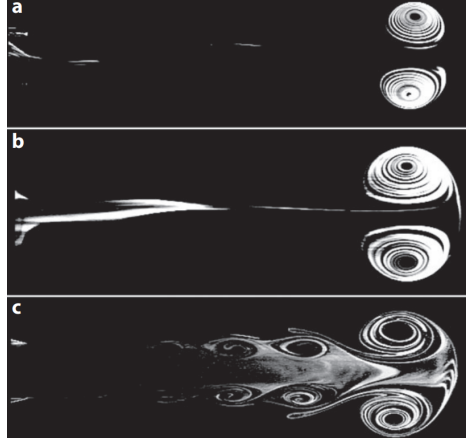


Figure 2.2: Visualization of vortex rings for (a)  $T = 2$ , (b)  $T = 3.8$ , (c)  $T = 14.5$  [4].

The purpose is to **maximize the size** of each generated vortex ring given the aforementioned constraint imposed by the dimensionless vortex formation time  $\hat{T}$ . Moreover, Krueger studied on the normalized time-averaged thrust per jet pulse, indicated with  $\hat{F}$  and he observed that maximizing the size of the vortex rings formed during propulsion, the efficiency of momentum transport is also optimized [4].

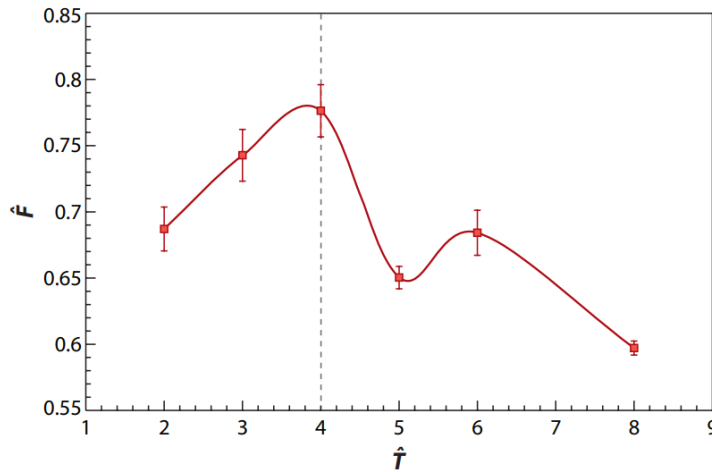


Figure 2.3: Normalized average thrust per pulse measurements [4].

### 2.2.3 Preliminary Studies

Historically, vortex ring formation has been most commonly studied using a **piston-cylinder apparatus**. In this configuration, a boundary layer of vorticity forms on the inner cylinder wall as the piston moves downstream inside the cylinder. At the downstream edge of the

cylinder, the boundary layer separates and rolls up into a vortex ring that propagates away from the vortex generator via self-induction.

Experimental research [3][4] has shown that the vortex formation number could be reduced by as much as 75% or increased by 35% by manipulating the temporal and spatial profiles of the cylinder exit velocity.

There are two mechanisms capable of extending the vortex ring growth process observed in piston cylinder experiments. The first method was to accelerate the trailing shear layer relative to the forming vortex ring so that the shear layer energy was sufficient to be accepted by the forming vortex ring and to consequently achieve a new steady vortex ring configuration and the second one was to increase the radial extent of the trailing shear layer.

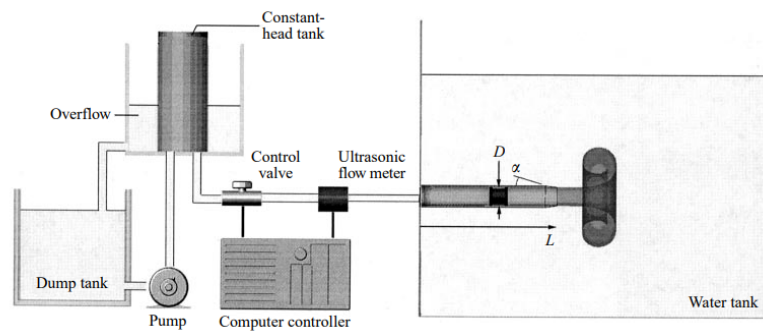


Figure 2.4: Example of a piston-cylinder apparatus used by Gharib [3].

In the example, vortex rings are generated by allowing the flow from the constant-head tank to drive a piston that pushes fluid out of a sharp-edged cylindrical nozzle into the surrounding fluid.

To sum up, numerical and experimental studies demonstrate the possibility of manipulating the limiting dimensionless vortex formation time from  $\hat{T} \approx 4$ . However, it does not appear possible to eliminate the limiting process altogether.

It's also important to say that there are cases in which the constant parameter  $C$  in equation (2.3) is manipulated via the dimensionless vorticity flux, so that limiting dimensionless vortex formation time  $\hat{T}$  can be changed from 4. Some examples will be discussed in subsequent chapters [3].



# Chapter 3

## Applications

### 3.1 Self-Propelled Vehicles Propulsion

It has been suggested that the generation of coherent vortical structures in the near-wake of a self-propelled vehicle can improve its propulsive efficiency by manipulating the local pressure field and entrainment kinematics.

We are going to observe a self-propelled underwater vehicle, designed with the capability to operate using either steady-jet propulsion or a pulsed-jet mode that features the roll-up of large-scale vortex rings in the near-wake.

Propulsion in air and water at high Reynolds numbers is typically studied by considering the mean flow created by the propulsor. In this steady flow approach, the thrust produced by the system is assumed to be dependent only on the mean velocity profiles upstream and in the wake of the propulsor.

Otherwise, removing the assumption of steady flow and allowing for spatiotemporal fluctuations of the fluid velocity and pressure, a richer parameter space becomes available to enhance propulsive efficiency.

So, vortex formation could determine **two main advantages** in terms of propulsion enhancement:

- It increases the generated thrust via the vortex overpressure in the near-wake
- It decreases the kinetic energy losses in the wake via vortex entrainment

#### 3.1.1 Analytical Model

Firstly, we recall from the known propulsion theory the classical expressions for Froude and Rocket efficiency,  $\eta_f$  and  $\eta_r$ , respectively:

$$\eta_f = \frac{2}{1 + \frac{U_w}{U_\infty}} \quad (3.1)$$

$$\eta_r = \frac{2}{\frac{U_\infty}{U_w} + \frac{U_w}{U_\infty}} \quad (3.2)$$

where  $U_\infty$  and  $U_w$  are the free-stream speed and average wake speed relative to the vehicle.



tify the relative contributions of vortex entrainment and added-mass to unsteady propulsion.

### 3.1.2 Experimental Setup and Methods

The chosen vehicle is 102.3 *cm* long with a maximum diameter of 15.2 *cm*. Its profile was inspired by a conventional submarine design, however, any attempt to improve the aerodynamic set-up of the vehicle was neglected.

In fact, priority was given to designing a vehicle that enables both steady and pulsed-jet propulsion with minimal changes to the configuration, so that the relative performance of the vehicle can be directly compared. A schematic diagram of the underwater vehicle studied in experiments is shown in figure (3.2).

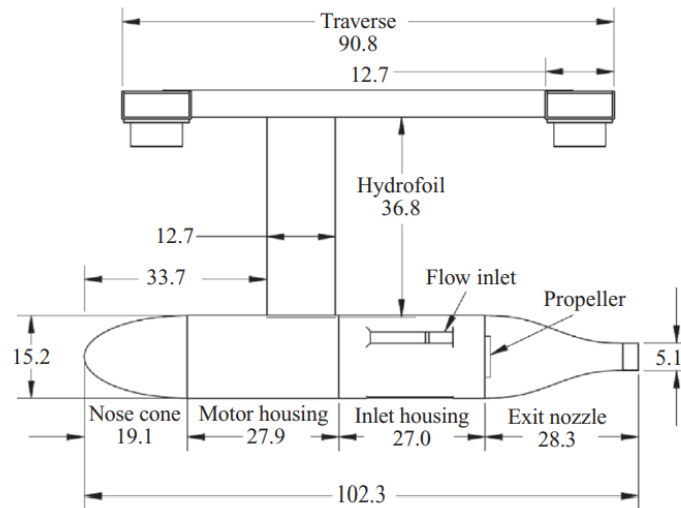


Figure 3.2: Schematic diagram of vehicle components including horizontal traverse [5].

The primary components of the vehicle are an anterior, water-flooded nose cone, waterproof motor housing with attached hydrofoil support strut, water-flooded inlet housing and a posterior exit nozzle connected to the inlet housing. Each of these components was constructed from glass-reinforced plastic.

The waterproof motor housing contains a 2hp DC motor<sup>1</sup> that drives the vehicle propeller. The voltage range for the motor is 24 – 36V with maximum continuous current of 35A. Electrical power is supplied to the motor from an external power supply via a flexible cable that passes through the hydrofoil support strut. Also, the motor throttle is regulated by a speed controller connected to the motor.

A symmetric vertical hydrofoil with approximately 13 % thickness is connected to the motor housing by epoxy, forming a waterproof seal. The hydrofoil provides the structural connection between the vehicle and a traverse that rolls along the horizontal rails of the water tank. Hence, the vehicle is constrained to unidirectional motion parallel to the rails of the water tank.

<sup>1</sup>AstroFlight Cobalt 60

Moreover, to modulate the steadiness of the jet efflux, a mechanism was designed to periodically occlude portions of the slots on the inlet housing. A planetary gear assembly connects the motor shaft to a hollow cylindrical shell that rotates inside the inlet housing. The outer surface of the rotating shell is flush with the inner surface of the inlet housing. As the shell rotates, the solid portion of the shell periodically blocks the inlet slots, preventing inlet flow and consequently throttling the exit flow. In this way, the rotational speed of the shell determines the level of inlet flow blockage and, by fluid continuity, the level of pulsation of the exit flow.

In order to verify that the pulsed-jet mode does indeed create large-scale coherent vortex rings in the near-wake, different types of measurements had been used:

1. PLIF measurements
2. DPIV measurements
3. LDV measurements

### Planar Laser-Induced Fluorescence measurements

Planar Laser-Induced Fluorescence (PLIF) is an optical measurement technique based upon fluorescence emitted from chemical species excited by planar laser light. Essentially a sheet of laser light is passed through a flow field, and the subsequent fluorescence relaxation event is captured on a digital camera.

In this experiment, the vehicle is held stationary by collar clamps, so that flow disturbances at the free surface are negligible. Then, Rhodamine 6G, a fluorescent dye of the order of hundreds of nanometers, is manually injected into a slot of the inlet housing. The output laser path involves the transmission of the laser beam through the free surface of the water. For the flow imaging a  $60mm$  lens video camera is used: then the image capture is triggered by a laser signal.

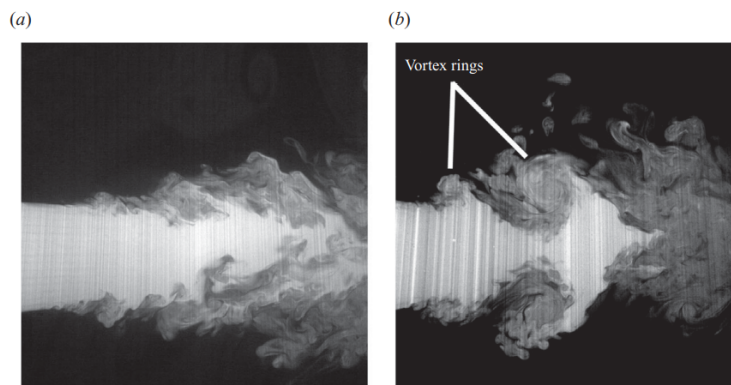


Figure 3.3: PLIF images of the near-wake of the vehicle during steady (a) and unsteady (b) propulsion [5].

## Digital Particle Image Velocimetry measurements

Laser based Digital Particle Image Velocimetry (DPIV) is a technique that allows for accurate measurement of an entire two-dimensional velocity field with no beam angulation. A DPIV measurement provides a more quantitative evaluation of the near-wake of the steady and pulsed-jet modes. Two lasers are fired with a relative time delay of  $5.3 - 21.2 \cdot 10^{-3} s$ , with smaller time delays at higher jet speeds to limit the displacement of particles between successive images.

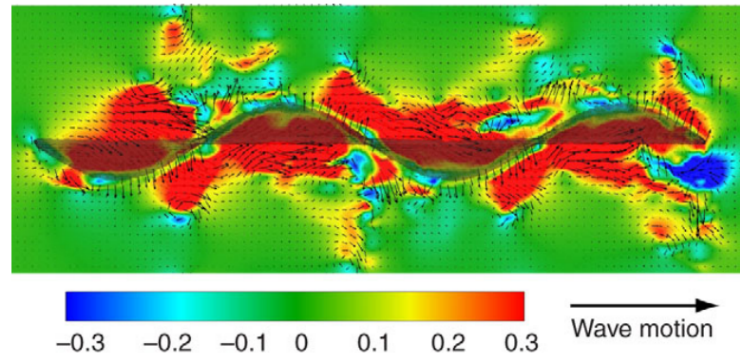


Figure 3.4: Typical output of a DPIV measurement [6].

For the flow imaging a  $60mm$  lens video camera is used in case of a steady jet, while bigger lens are used in case of an unsteady one. Particle images were processed using an in-house DPIV code. Once it is evident that the pulsed-jet configuration produced vortex ring roll-up in the near-wake as designed, the  $60 mm$  lens and associated DPIV processing parameters are used to verify the axial symmetry of the vortex rings by measuring the full wake width.

## Laser Doppler Velocimetry measurements

Laser Doppler Velocimetry (LDV) is a technique used to measure the instantaneous velocity of a flow field. It's non-intrusive and can measure all the three velocity components. The laser Doppler velocimeter sends a monochromatic laser beam toward the target and collects the reflected radiation. According to the Doppler effect, the change in wavelength of the reflected radiation is a function of the targeted object's relative velocity.

In the experiment LDV is used to measure the mean velocity profiles in the near-wake during steady and unsteady self-propulsion. Since LDV is a pointwise technique, the spatial velocity profiles were constructed from repeated tests of the vehicle.

In order to do that, an aluminium probe strut is designed to mount the LDV at the rear of the vehicle traverse. The probe strut was attached to a  $100 mm$  vertical translation stage which is mounted to an horizontal stage, thus allowing LDV probe volume to translate in the vertical and horizontal direction as it is shown in figure (3.5). At the end, LDV measurement data were transferred in real-time to a PC, which automatically followed behind the vehicle at a fixed distance.

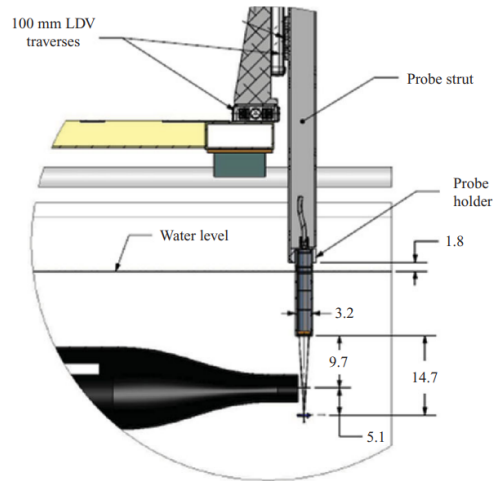


Figure 3.5: LDV assembly mounted onto the vehicle traverse [5].

### 3.1.3 Enhancement on Vehicle Performance

Froude efficiency versus motor speed has been measured for the various steady and unsteady self-propelled vehicle configurations.

Results show that at low motor speeds, steady-jet propulsion created by the rotating cylindrical shell is inferior to steady propulsion in the absence of the rotating shell. The performance of the steady jet with rotating shell does improve with increasing motor speed, but it does not exceed the baseline performance of the steady jet without rotating shell. This result is expected given that the steady-jet propulsion systems are functionally equivalent. In contrast, the unsteady propulsor consistently outperforms the baseline steady propulsor in terms of Froude efficiency. Increases in efficiency exceeding 40 % are achieved, with modest decreases in the propulsion enhancement at higher motor.

In terms of hydrodynamic efficiency, the magnitude of vortex enhancement of propulsion is even greater, exceeding 70 % improvement over baseline steady propulsion.

In both cases, modest decreases in vortex enhancement are observed at higher motor speeds.

This study demonstrates of a net **reduction in power consumption** of the **unsteady propulsor**, accounting for the power required to create flow unsteadiness. Despite the inevitable shortcomings of the vehicle design, such as hydrodynamic losses within the inlet housing and the propeller unapt to the unsteady inflow conditions, the results make clear the potential benefits of vortex-enhanced propulsion [5].

## 3.2 Biologic Propulsion Mechanisms

Fishes swim by flapping their tail and other fins. They optimize both their steady swimming efficiency and their ability to accelerate and turn by producing an individual optimal ring with each flap of the tail or fin. Other sea creatures, such as squid and salps, eject a volume of fluid through a rear orifice, producing vortex rings which are also optimal.

In both cases the **vortices roll up** into three-dimensional ring-like structures. Previous theoretical studies and observations have made good progress towards the understanding of both these mechanisms, and what constitutes optimal swimming behaviour.

Two definitions of swimming efficiency are commonly used: the first is purely mechanical and relates the flow round and behind the body to the mean thrust this produces, while the second has a biological component and considers the energy supplied by the muscles and the resulting swimming speed.

We will take into account the first one, discussing about efficiency in terms of thrust achieved for a given amount of work. In addition to that, to allow an accurate analysis, we will resume the Linden&Turner theory [7]: when vortex rings are produced by ejecting a length  $L$  of fluid from a circular pipe of diameter  $D$ , it could be observed that the maximum length of a plug of fluid ejected from the pipe is given by  $L/D = 4$ . For larger  $L/D$ , secondary vortices formed in the wake behind the leading vortex. In the end, this theory predicts a maximum value of  $L/D = 3.5$ , close to the observed value  $L/D = 4$ .

Moreover, we can consider the **cost of locomotion**, defined as the energy required per unit mass to propel a body a unit distance and values for different species could be observed in table (3.1). From the figures is evident that the swimming of squid is pretty inefficient and that salps do well even when compared with fishes.

<b>Animal</b>	<b>Cost of locomotion</b> $\left[\frac{J}{kg \cdot m}\right]$
Squid	7.6 – 12.6
Salp	0.6 – 2.1
Salmon	1.9

Table 3.1: Different species cost of locomotion according to Madin (1990) [8].

### 3.2.1 Squids, Jellyfish and Salps

The mode of swimming adopted by aquatic creatures that is most directly related to the flow of fluid from a pipe is that which produces a backward-directed jet or pulse, commonly called jet propulsion. So, the question is how long a jet provides the optimal efficiency.

Expressing the above comparison in a different way, it is possible to state that the squid and the heaviest sockeye salmon share approximately the same mass, optimum swimming velocity and body length, but the squid, using jet propulsion, needs more than five times

as much energy [7].

Measurements obtained from Johnson et Al [9] on squid showed that typically 200 ml of water is expelled in 0.2s through an orifice of area  $1.5\text{cm}^2$ . This implies a velocity of 600 cm/s and a jet 120 cm long, so that  $L/D = 87$ .

**Salps pump water by muscular action** through their tubular bodies. They have orifices at both ends; they take in water at the front, and eject it at the back with the front opening closed, so that they can achieve more nearly steady swimming than other jet producing creatures. That process is illustrated in the figure (3.6), in which the passage of a single pulse is made visible with uranine dye and recorded on videotape, so that the formation and progress of a vortex ring is clearly seen.

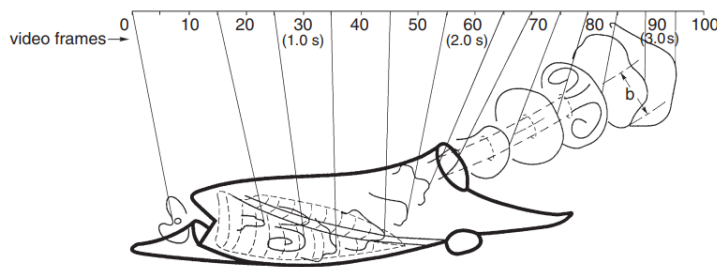


Figure 3.6: The water flow through a salp [7].

From the data tabulated in the Bone and Trueman (1983) [10] paper we can deduce that  $L/D$  for the ejected plugs lies in the range of 10 – 20 for various species of salp. Other authors have also estimated  $L/D$  for salps, but the observations they have used are poorly constrained, because both the area of the exit opening and the pulse length are not known very accurately, and the values given vary over a wide range. In the end, the value suggested is around  $L/D = 6.7$ , slightly longer than the optimum we have derived.

Instead, the mechanics of jellyfish jet propulsion is characterized by the ‘bell’ of a typical jellyfish, which is roughly hemispherical, with a height of 1 cm and a diameter of 2 cm, with a ring of tissue around the opening restricting it to half the bell area. This ratio is very sensitive to the diameter of the opening, which is poorly known. For example  $D = 1\text{ cm}$  implies  $L/D = 2.67$ , while  $D = 0.85\text{ cm}$  gives  $L/D = 4.35$ .

In conclusion, jellyfish are significantly less efficient than salps, because fluid is both drawn in and ejected through the same rear opening, and there is a large acceleration reaction that contributes to the drag as the velocity and mass change during the cycle.

### 3.2.2 Fish

Most marine organisms have only discrete mechanisms at their disposal, and cannot generate a continuous jet. Fishes swim by oscillating their pectoral fins or by passing a wave of curvature backwards along the body, shedding vorticity from the caudal fin into the wake, which rolls up into three dimensional ring-like structures.

The quantitative study of fish wakes has been transformed recently by the use of digital particle image velocimetry (DPIV) to visualize and measure the water flow pattern in the wake of the body and fins. Sheets of laser light orientated in various directions are used to

illuminate small particles seeded into a recirculating flow tank, in which the fish is swimming at a fixed position relative to the light beams.

**Pectoral fin wakes** There is no direct measure of a ‘plug length’ or  $L/D$  for pectoral-fin swimming, so we must use another property of the vortices produced to compare them with the proposed optimal condition. In several cases the radius  $R$  of the ring and the radius  $R_0$  of the mean vortex-core have been measured. The ratio  $R_0/R$  is in fact close to a parameter  $\epsilon$  which has a one-to-one correspondence with  $L/D$ . According to the Linden&Turner theory, the maximum dimensionless plug length corresponds to a core-to-ring radius ratio of  $\epsilon = 0.42$ .

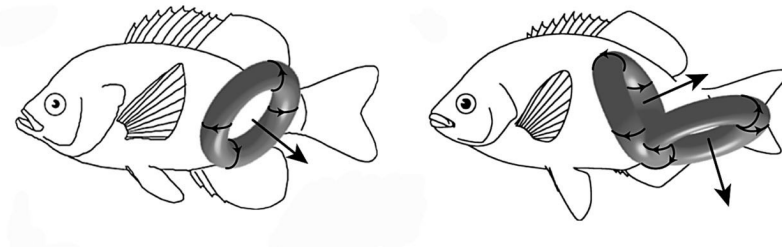


Figure 3.7: Vortex wakes of two different swimming fishes produced with pectoral fins [7].

Experimental measurements [7] has shown that the vortex ring at the end of the stroke of the fin had  $R = 1.8 \text{ cm}$  and a mean  $R_0$  of  $1.1 \text{ cm}$ , so that  $\epsilon = R_0/R = 0.61$ , a little larger than our theoretical optimal value.

**Caudal Fin wakes** Direct measurements of the flow around and behind various species of fish using DPIV. These proto-vortices are shed when the inflection points reach the tail. The vortices produced by the tail itself are shed when the tail changes direction. The fish can vary the phase of the shedding, and hence the shape of the wake and the contribution to thrust of the body vortices. For mullet, for example, less than half the thrust is caused by the body; the tail produces most of the thrust as well as controlling the vorticity shed from the body.

A chain of rings is produced in the wake, with the momentum directed away from the

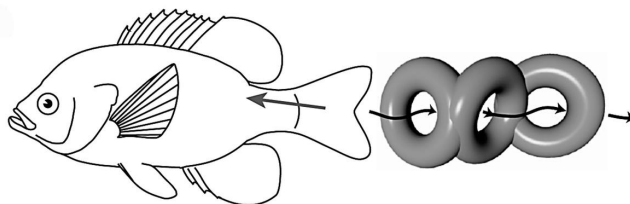


Figure 3.8: Lateral view of sunfish swimming with the caudal fin [7].

mean path of motion rather than directly backwards, as it is in a jet expelled from a body

cavity, like in figure (3.6).

There is a relationship between Strouhal Number and the plug aspect ratio:

$$\frac{L}{D} = \frac{1}{St}$$

A wide variety of fishes swim with  $St$  in the range of 0.25 – 0.35, corresponding to an  $L/D = 3 - 4$ , and it has been concluded that this value has evolved as the most efficient repetition rate for the production of thrust.

### 3.2.3 Measurements

DPIV in vertical and horizontal planes through the fish body was used to determine velocity vectors and other parameters in the flow behind the fish. It showed that the wake consists of a **series of strong counter-rotating elliptical vortices**, linked together as vortex loops rather than separate.

The ellipses are larger and more elongated at the higher speed. Using the vorticity data, the ring radius  $R$  to the centre of the core and the mean vortex-core radius  $R_0$  (along with other ring properties) were calculated and tabulated. The forces produced by the rings have been calculated: these are directed laterally at an angle to the wake, so that the effective forward thrust is about one-third of that calculated from the properties of the individual rings.

DPIV has also been used to measure the properties of vortices produced by starting and turning manoeuvres of fishes, and shows that continuous periodic shedding is not essential for the efficient production of thrust. In fact, for a fish making a sharp turn, the bending of the body is followed by a double stroke of the tail, which forms a vortex generated first by the body, with the tail fin adding to the shed momentum. The controlled release of vorticity into the wake provides thrust in the new swimming direction [7].

### 3.3 Blood Flow in the cardiac left ventricle

Heart disease remains a leading cause of death worldwide. Previous research has indicated that the dynamics of the cardiac left ventricle (LV) during diastolic filling may play a critical role in dictating overall cardiac health.

So, the aim is to demonstrate that major aspects of cardiac function are reflected uniquely and sensitively in the optimization of vortex formation in the blood flow during early diastole, as measured by a dimensionless numerical index. This index of optimal vortex formation correlates well with existing measures of cardiac health such as the LV ejection fraction.

Moreover, vortex dynamics immediately reflect physiological changes to the surrounding system, and can provide early indications of long-term outcome. Intracardiac flow analysis is useful in evaluating the current disease status, selection of treatment strategy, assessment of response to therapy, and prediction of future clinical outcomes in patients with heart failure (HF). Therefore, **vortex flow analysis** may contribute to the optimal management of patients with heart failure.

#### 3.3.1 Results

To quantify the process of vortex ring formation and its potential optimization, a quantitative index is required. The index is most useful if it is dimensionless, so that it can be compared across patient groups. Existing dimensionless measures of cardiac health, such as the ratio index of diastolic blood flow, cannot be interpreted without considering patient-specific effects.

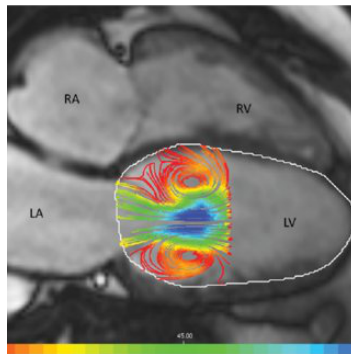


Figure 3.9: Three-dimensional in-vivo intra-cardiac vortex flow [11].

A dimensionless numerical index has been previously defined with (2.3) to characterize vortex rings formed by fluid ejected from a rigid tube. In effect, the vortex formation time is a measure of the length-to-diameter ratio of the ejected fluid column. As said before, vortex ring will continue to grow larger during the process of fluid transport until a vortex formation time  $T \approx 4$  is reached. After this point, the vortex ring is unable to grow larger because of energetic constraints and ejected fluid subsequently forms a trailing jet behind the vortex ring. Therefore, vortices are optimized for efficient fluid transport when formed during a vortex formation time  $T \approx 4$ . In the left heart, blood flow from the atrium to the ventricle passes the mitral valve leaflets, which form a time-varying exit diameter

$D(t)$  as opposed to the constant diameter studied in the experiments noted above and in numerical simulations. The effect of a time-varying exit diameter on the vortex formation process was recently studied in vitro [11], like in figure (3.9) and it was shown that for temporal increases in exit diameter, the vortex formation time corresponding to maximum vortex growth remains unchanged at  $T \approx 4$ .

During normal LV function, the E wave<sup>2</sup> phase is completed within a vortex formation time  $3.3 < T < 5.5$ . This range is consistent with the optimal range of vortex formation time found in previous in vitro vortex formation studies and, interestingly, also has been identified as the optimal range of vortex formation for aquatic locomotion, as we have seen in the previous section.

In further support of these results, two independent studies were conducted in the Division of Cardiology at the University of California at San Diego and in the Division of Engineering and Applied Science at the California Institute of Technology. A total of 110 volunteers from 5 to 84 years of age were randomly selected to undergo transthoracic echocardiography for imaging the left ventricle from the apical view.

The results are shown in the graph:

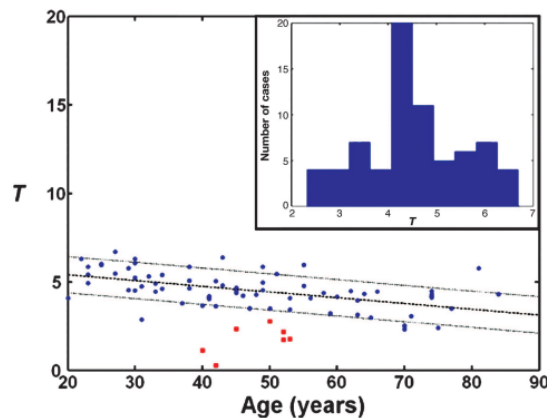


Figure 3.10: Vortex formation time in adult humans from blind test and those with DCM [11].

Blue circles indicate the calculated values of vortex formation time for blind test cases where no prior information about patients' cardiac health was obtained, and red squares indicate the data for patients with DCM (Dilated Cardiomyopathy).

It is evident that the distribution of vortex formation times corresponding to the DCM patients is located below the optimal range, as predicted by the aforementioned relationship between vortex formation time and ejection fraction.

### 3.3.2 Methods

In order to evaluate the LV diastolic filling event and its relationship with cardiac function, the set of parameters required to determine the dimensionless vortex formation time  $\hat{T}$

<sup>2</sup>Peak velocity blood flow from left ventricular relaxation in early diastole

were recorded. The mitral annulus diameter was used as the exit diameter, and was measured from long-axis apical views of the LV at the peak of diastole thanks to Doppler images. Then, mean blood flow velocity from the atrium to the ventricle of the left heart was obtained from pulsed-wave Doppler measurements in the immediate downstream vicinity of the opened.

To sum up, considering (2.3), in this case the terms are:

- $U$ , the mean blood flow velocity
- $D$ , the mitral annulus diameter
- $T$ , the duration of the E wave

The next step is find a relationship between LV vortex formation time and the LV ejection fraction. First of all, the term ejection fraction (EF) refers to the ratio of LV stroke volume to the LV volume at the end of diastole:

$$EF = \frac{EDV - ESV}{EDV} = \frac{SV}{EDV}$$

where:

- EDV is the LV volume at the end of diastole (LV filling)
- ESV is the LV volume at the end of systole (LV ejection)
- SV is the stroke volume

Denoting  $\beta$  as the fraction of the stroke volume contributed from LV A wave<sup>3</sup> filling (equal to 0.2 in a normal heart at rest) and defining a LV geometry parameter  $\alpha$  as:

$$\alpha = \frac{EDV^{\frac{1}{3}}}{D}$$

we get the equation we were searching for:

$$\hat{T} = \frac{4(1 - \beta)}{\pi} \alpha^3 EF \quad (3.4)$$

---

<sup>3</sup>Peak velocity flow in late diastole caused by atrial contraction



# Chapter 4

## Discussion

### 4.1 Outlook

It is possible to state that the concept of optimal vortex formation, especially applied to vortex dynamics or even to biological propulsion, is still far from reaching a definitive and satisfactory conclusion.

The existing data suggest that the concept of optimal vortex formation does indeed extend to these more complex cases; however, as shown above, changes in vortex generator geometry affect the specific value of dimensionless time  $\hat{T}$  at which vortex growth is limited. The ability to predict the optimal vortex formation time for arbitrary vortex generator geometries will inform the search for its occurrence in measurements of biological propulsion systems. No two biological propulsion systems function identically, even systems of the same species and age. Similarly, we can also expect cycle-to-cycle variations in vortex formation within that same propulsor.

As discussed above, laboratory measurements indicate variations of up to 15% in the optimal dimensionless vortex formation time during their experiments. It is currently unknown how close to the nominal optimal vortex formation time a system must operate to maintain the associated performance benefits.

### 4.2 Pros and Cons

The advantages have been explained in the previous chapters and these are evident in terms of improving the characteristics of the flows. However, the studies are **not yet at a sufficiently advanced level** that we can blindly rely on this type of analysis: this is even more evident if we think about the application related to blood flow in the cardiac left ventricle. In fact, diagnosis of left heart failure provides a poignant example in which natural variability must not be mistaken for suboptimal performance lest false positive indications of cardiac dysfunction arise.

Moreover, in the field of bio-inspired propulsion, it is useful to know to what degree design objectives that compete with the achievement of the optimal vortex formation time can be accommodated, and to what degree that optimum can be maintained in the face of unknown design variables.

### 4.3 Recommendations of Future Work

Given current limitations in our ability to measure three dimensional flows experimentally, computational tools can provide valuable insight into the process of optimal vortex formation. Furthermore, large parametric studies aimed at determining the functional dependence of the dimensionless vortex formation time on the propulsor design can be accomplished *in silico* with less expense than an equivalent experimental study.

In summary, the concept of optimal vortex formation not only provides a unifying framework in which to understand biological propulsion, it also suggests an objective metric with which to design and evaluate engineered propulsion systems. To exploit the concept of optimal vortex formation for the greatest advantage to the engineer and biologist, we must improve our understanding of the governing physical principles of optimal vortex formation. Therefore, in this sense, it is reasonable to expect that these recent studies may be the basis for building something really important in the years to come, through the **implementation of new technologies** and a consequent deeper knowledge of the mechanisms that regulate the phenomenon.

In this way it will be possible to convert the disadvantages into advantages and obtain a powerful tool for the scientific community.

# Bibliography

- [1] Helmholtz H. “Über Integrale der hydrodynamischen Gleichungen, welche den Wirbelbewegungen entsprechen”. In: *Journal für die reine und angewandte Mathematik* 55 (1858), pp. 25–55. doi: <https://doi.org/10.1515/crll.1858.55.25>.
- [2] Houbraken M. *The effect of formulation on the volatilisation of plant protection products*. UGent - Faculty of Bioscience Engineering, 2018. ISBN: 9780198520115.
- [3] M. Gharib et al. “A universal time scale for vortex ring formation”. In: *Journal of Fluid Mechanics* 360 (1998), pp. 121–140. doi: <https://doi.org/10.1017/S0022112097008410>.
- [4] John O.Dabiri. “Optimal Vortex Formation as a Unifying Principle in Biological Propulsion”. In: *Annual Review of Fluid Mechanics* 41 (2008), pp. 17–33. doi: <https://doi.org/10.1146/annurev.fluid.010908.165232>.
- [5] Lydia A. Ruiz, Robert W. Whittlesey, and John O.Dabiri. “Vortex-enhanced propulsion”. In: *Journal of Fluid Mechanics* 668 (2011), pp. 5–32. doi: <https://doi.org/10.1017/S0022112010004908>.
- [6] Shirgaonkar A. et al. “The hydrodynamics of ribbon-fin propulsion during impulsive motion”. In: *Journal of Experimental Biology* 211 (2008), pp. 3490–3503. doi: <https://doi.org/10.1242/jeb.019224>.
- [7] P.F. Linden and J.S. Turner. “‘Optimal’ vortex rings and aquatic propulsion mechanisms”. In: *Proceedings of the Royal Society B: Biological Sciences* 271 (2004), pp. 647–653. doi: <https://doi.org/10.1098/rspb.2003.2601>.
- [8] Madin L. P. “Aspects of jet propulsion in salps”. In: *Canadian Journal of Zoology* 68 (1990), pp. 765–777. doi: <https://doi.org/10.1139/z90-111>.
- [9] Johnson W., Soden P. D., and Trueman E. R. “A study in jet propulsion: an analysis of the motion of the squid”. In: *Journal of experimental biology* 56 (1972), pp. 155–165. doi: <https://doi.org/10.1242/jeb.56.1.155>.
- [10] Q. Bone and Trueman. “Jet propulsion in salps (Tunicata: Thaliacea)”. In: *Journal of Zoology* 201 (1983), pp. 481–506. doi: <https://doi.org/10.1111/j.1469-7998.1983.tb05071.x>.
- [11] M. Gharib et al. “Optimal vortex formation as an index of cardiac health”. In: *Proceedings of the National Academy of Sciences (PNAS)* 103 (2006), pp. 6305–6308. doi: <https://doi.org/10.1073/pnas.0600520103>.